

Isospin-Violating Dark Matter at the LHC

Kaoru Hagiwara^a, Danny Marfatia^b, Toshifumi Yamada^{a,c}

^a *KEK Theory Center and SOKENDAI,
1-1 Oho, Tsukuba, Ibaraki 305-0801, Japan*

^b *Department of Physics & Astronomy, University of Kansas, Lawrence, KS 66045, USA*

^c *Department of Physics, University of Tokyo,
7-3-1 Hongo, Bunkyo-ku, Tokyo 113-0033, Japan*

Abstract

We consider a toy model of dark matter (DM) with a gauge singlet Dirac fermion that has contact interactions to quarks that differ for right-handed up and down quarks. This is motivated by the isospin-violating dark matter scenario that was proposed to reconcile reported hints of direct DM detection with bounds from non-observation of the signal in other experiments. We discuss how the effects of isospin violation in these couplings can be observed at the LHC. By studying events with large missing transverse momentum (\cancel{E}_T), we show that the ratio of mono-photon and mono-jet events is sensitive to the difference in the absolute values of the couplings to the up and down quarks, while a dedicated study of di-jet plus \cancel{E}_T events can reveal their relative sign. Our methods have broad applicability to new physics that involves unequal couplings to up and down quarks.

1 Introduction

Once a hint of dark matter (DM) is found in events with large missing transverse momentum (\cancel{E}_T) at the LHC, the next task will be to study how the DM particle couples to standard model (SM) particles. It can be the case that the DM particle couples to up and down quarks differently. Observing such an isospin violating feature of the new physics sector would give an important clue for the determination of the Lagrangian of the underlying theory. Also, it is itself a challenge in the physics of hadron colliders, requiring elaborate kinematical cuts to extract information from parton-level processes.

In this context, isospin-violating dark matter (IVDM) [1] provides a scenario in which a DM particle does not couple identically to up and down quarks. This model was motivated by DM direct detection experiments. The DAMA [2] and CoGeNT [3] experiments observed signals that are potentially of dark matter origin. The signals are consistent with a DM particle of mass 10 GeV scattering off nuclei with a spin-independent nucleon cross section of $\sigma_N \sim 2 \times 10^{-4}$ pb and $\sigma_N \sim 7 \times 10^{-5}$ pb, respectively. However, the XENON [4] and CDMS [5] experiments reported negative results. To accommodate the apparently inconsistent data, the authors of Ref. [1] considered a dark matter particle that couples to up and down quarks differently. Then the cross section of dark matter scattering off protons differs from that off neutrons, and the apparent tension among dark matter direct detection experiments is attributed to the different proton-neutron ratios of the detector materials.

We study the possibility of testing the scenario at the LHC by measuring the couplings to up and down quarks. We work in a general context and simply assume that a new stable particle that is a singlet under the SM gauge group (called “dark matter” in the following) couples to right-handed up and down quarks with different strengths and signs. At the LHC, the production of DM particles associated with a jet(s) or photon gives rise to events with a hard jet(s) or photon plus large missing transverse momentum (\cancel{E}_T). Since the up and down quarks couple differently to the photon but identically to the gluons, the magnitudes of the two couplings can be measured by comparing the cross section of the mono-jet plus \cancel{E}_T signal with that of the mono-photon plus \cancel{E}_T signal. The relative sign of the dark matter couplings is more difficult to measure because it requires the measurement of the interference between the dark matter coupling to the up quark and that to the down quark. This is possible through the subprocess, $ud \rightarrow ud + DM DM$, but the interference effects need to be identified in the presence of the other dijet+ $DM DM$ subprocesses and the SM backgrounds.

Our discussion of how isospin-violating couplings of a DM particle can be studied at the LHC involves several ingredients. We use MadGraph 5 [6] for calculating matrix elements and for generating DM signal events, Pythia 8 [7] for parton showering, and PGS 4 [8] for simulating

detector effects. The outline of the paper is as follows. In Section 2, we describe our toy model of IVDM. In Sections 3, 4 and 5, we investigate the DM signals from three channels, mono-jet plus \cancel{E}_T , mono-photon plus \cancel{E}_T , and di-jet plus \cancel{E}_T . In Section 6, we compare the signals from the three channels and study signatures of isospin violation in the matter-DM couplings.

2 Model

We consider a toy model in which a DM particle couples to quarks with isospin-violating couplings. We introduce a Dirac fermion χ that is a singlet under the SM gauge group. It couples to the up and down quarks through vector-like and axial vector-like contact interactions. The relevant part of the Lagrangian is

$$\mathcal{L}_{DM} = i\bar{\chi}\gamma^\mu\partial_\mu\chi - m_\chi\bar{\chi}\chi + \frac{1}{\Lambda^2}(g_Q\bar{q}_L\gamma_\mu q_L + g_U\bar{u}_R\gamma_\mu u_R + g_D\bar{d}_R\gamma_\mu d_R)(\bar{\chi}\gamma^\mu\chi), \quad (1)$$

where Λ denotes the energy scale of the contact interaction and q_L denotes the SU(2) doublet of left-handed up and down quarks. For $g_U \neq g_D$, χ is IVDM.

At the LHC, we would like to extract the magnitudes and relative signs of the couplings, g_U , g_D and g_Q . In the following, we examine the possibility of measuring g_U/g_D by setting $g_Q = 0$. Implications of $g_Q \neq 0$ will be discussed in the last section.

3 Mono-jet + \cancel{E}_T

In this section, we study events with a high p_T mono-jet and large \cancel{E}_T , which is the discovery channel for a DM particle at hadron colliders. We first focus on the case of pp collisions at $\sqrt{s} = 7$ TeV and reproduce the results of Ref. [9]. We then consider $\sqrt{s} = 14$ TeV, the target energy of the LHC. By optimizing the selection cuts, we estimate the DM signal for various values of g_U/g_D for a fixed value of $\sqrt{g_U^2 + g_D^2}$ and $g_Q = 0$.

3.1 Study for $\sqrt{s} = 7$ TeV

Following Ref. [9], we adopt the *veryHighPT* cut of the ATLAS search [10], which yields the most stringent bound on the DM-quark interactions. This cut is described by

- Require $\cancel{E}_T > 300$ GeV.
- Highest p_T jet satisfies $|\eta_1| < 2.0$ and $p_{T1} > 350$ GeV.

- Event is vetoed if the second hardest jet satisfies $|\eta_2| < 4.5$, and $p_{T2} > 60$ GeV or $\Delta\phi(\vec{p}_{T2}, \vec{\cancel{E}}_T) < 0.5$.
- Event is vetoed if there is another jet that satisfies $|\eta| < 4.5$ and $p_T > 30$ GeV.
- Event is vetoed if there is an electron that satisfies $|\eta_e| < 2.47$ and $p_{Te} > 20$ GeV.
- Event is vetoed if there is a muon that satisfies $|\eta_\mu| < 2.4$ and $p_{T\mu} > 10$ GeV.

The dominant sources of background for mono-jet events that satisfy the above criteria are $Z + \text{jet}$ events with $Z \rightarrow \nu\nu$, and $W + \text{jet}$ events with $W \rightarrow \tau\nu$ or $W \rightarrow l\nu$ ($l = e, \mu$) where the τ decay products or leptons do not satisfy any of the veto criteria.

We estimate the $Z + \text{jet}$ background by first generating $Z(\rightarrow \nu\nu) + 1, 2$ jets events at the matrix element level [6] with precuts $\cancel{E}_T > 200$ GeV and $k_T > 140$ GeV for the jets. We next simulate parton showering [7] by using the k_T -jet matching scheme [11] to match the p_T distribution of the second hardest jet simulated via the parton showering of $Z + 1$ jet events and the distribution calculated from the matrix elements of $Z + 2$ jets events. The matching scale is set at 200 GeV. We have confirmed that the cross section after the final cut does not change significantly when the matching scale is varied by ± 60 GeV around 200 GeV. Finally, we perform a detector simulation [8] and the cross section for $Z(\rightarrow \nu\nu) + \text{jets}$ events that pass the *veryHighPT* cut is found to be

$$\sigma_{Z(\rightarrow \nu\nu)+\text{jets}}(\text{veryHighPT}) \simeq 106 \text{ fb}. \quad (2)$$

In a similar manner, we generate $W + 1, 2$ jets events in which W decays into $\tau\nu_\tau$ and those in which W decays into $e\nu_e$ or $\mu\nu_\mu$, at the matrix element level with the precuts $p_T^l > 200$ GeV, where p_T^l denotes the transverse momentum for the three-momentum sum of the lepton momenta, and $k_T > 140$ GeV for the jets. We then simulate parton showering with a matching scale of 200 GeV, and study the detector effects. Again, we have confirmed that the cross section after the final cut does not change much when the matching scale is varied around 200 GeV by ± 60 GeV. The cross sections for $W(\rightarrow \tau\nu_\tau) + \text{jets}$ events and $W(\rightarrow e\nu_e/\mu\nu_\mu) + \text{jets}$ events that pass the *veryHighPT* cut are found to be

$$\sigma_{W(\rightarrow \tau\nu_\tau)+\text{jets}}(\text{veryHighPT}) \simeq 35.4 \text{ fb}, \quad (3)$$

$$\sigma_{W(\rightarrow e\nu_e/\mu\nu_\mu)+\text{jets}}(\text{veryHighPT}) \simeq 22.2 \text{ fb}. \quad (4)$$

In Table 1, we compare the numbers of background events estimated in Eqs. (2-4) with those estimated by the ATLAS collaboration [10] for an integrated luminosity of 1 fb^{-1} . We find satisfactory agreement. Following Ref. [9], we normalize our estimates for $Z + \text{jets}$ events

Background	Our simulation	ATLAS collaboration	Normalization factor
$Z(\nu\nu) + \text{jets}$	106	$124 \pm 12 \pm 15$	1.17
$W(\tau\nu) + \text{jets}$	35.4	$36 \pm 7 \pm 8$	1.08
$W(e/\mu\nu) + \text{jets}$	22.2	$26 \pm 4 \pm 3$	

Table 1: The numbers of background events that pass the *veryHighPT* cut for 1 fb^{-1} LHC (at 7 TeV) according to our simulation (see Eqs. 2-4), compared to the estimates by ATLAS [10]. The last column gives the ratios of the ATLAS estimate to our estimate.

and for $W + \text{jets}$ events to those of the ATLAS collaboration. The normalization factors are also shown in Table 1. Note that the normalization factor for the $Z(\nu\nu) + \text{jets}$ background (1.17) is consistent with Ref. [9], where it is estimated to be 1.2.

The DM signal in mono-jet events arises mainly from the following subprocesses:

$$g u \rightarrow u \chi \bar{\chi}, \quad (5)$$

$$g d \rightarrow d \chi \bar{\chi}. \quad (6)$$

We simulate the DM contribution to mono-jet events by following the method we have adopted for the background simulations. We generate $pp \rightarrow \chi\bar{\chi} + 1, 2 \text{ jets}$ events at the matrix element level with the precuts $\cancel{E}_T > 200 \text{ GeV}$ and $k_T > 140 \text{ GeV}$ for the jets. Parton showering is simulated with a 200 GeV matching scale, and detector effects are simulated. We have also confirmed for the DM signal that the final results are not significantly affected by varying the matching scale around 200 GeV. Finally, we rescale our signal by a factor of 1.17; see Table 1.

In order to compare our results with those of Ref. [9], we estimate the DM signal with $\Lambda = 400 \text{ GeV}$, $g_U = g_D = g_Q = 1$ and $m_\chi = 10 \text{ GeV}$. We show the \cancel{E}_T distribution in Fig. 1. All the curves are in good agreement with those in Fig. 2 of Ref. [9]. The difference in the 300-350 GeV bin is likely due to the different modeling of parton showers.

To compare the lower bound on Λ from our analysis with that from Ref. [9], we derive the observed bound for $m_\chi = 10 \text{ GeV}$ and $g_U = g_D = g_Q = 1$. It should be noted that only when all three couplings of the effective Lagrangian in Eq. (1) are equal, do we have purely vector-like couplings for both up and down quarks, as assumed in Ref. [9]. Isospin violation with purely vector-like couplings is not compatible with electroweak symmetry. To place 90% C.L. lower limits on Λ we require [9]

$$\chi^2 \equiv \frac{(N_{obs} - N_{DM}(\Lambda) - N_{SM})^2}{N_{DM}(\Lambda) + N_{SM} + \sigma_{SM}^2} < 2.71, \quad (7)$$

where N_{obs} , N_{DM} and N_{SM} are the number of observed events, the expected number of signal events, and the SM expectation, respectively, and σ_{SM} is the uncertainty in N_{SM} . We adopt

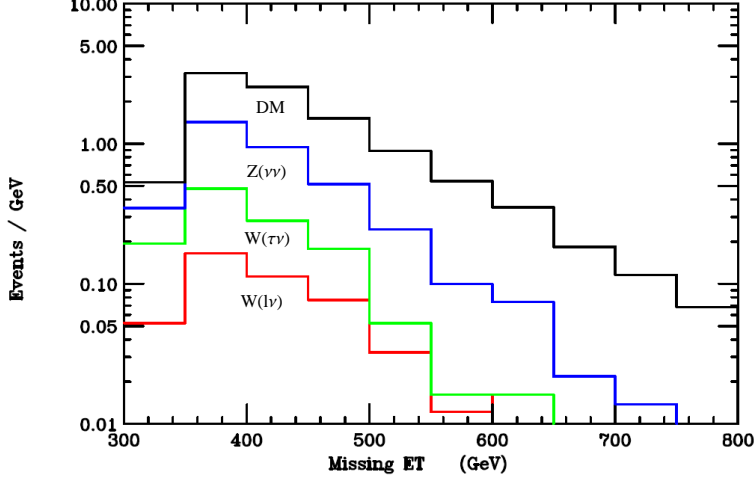


Figure 1: The \cancel{E}_T distribution of the backgrounds and the DM signal for 1 fb^{-1} at ATLAS. The curves from bottom to top successively include the $W(e/\mu\nu) + \text{jets}$ background, the $W(\tau\nu) + \text{jets}$ background, the $Z(\nu\nu) + \text{jets}$ background, and the DM signal with $\Lambda = 400 \text{ GeV}$ and $m_\chi = 10 \text{ GeV}$. *i.e.*, the curve labelled “DM” corresponds to the sum of all the backgrounds and the DM signal.

$N_{obs} = 167$ and $N_{SM} \pm \sigma_{SM} = 193 \pm 25$ as obtained by the ATLAS collaboration in 1 fb^{-1} of data. After rescaling, we find the number of signal events for $\Lambda = 400 \text{ GeV}$ to be $N_{DM} = 319$, which implies: $N_{DM}(\Lambda) = 319 \times (400 \text{ GeV} / \Lambda)^4$. Finally, using the criterion Eq. (7), we obtain the 90% C.L. bound,

$$\Lambda > 783 \text{ GeV} . \quad (8)$$

On the other hand, Fig. 4 of Ref. [9] shows separate bounds on Λ for DM-up quark and DM-down quark interactions, which are both purely vector-like. These bounds can be translated into a bound on Λ for $g_U = g_D = g_Q = 1$:

$$\Lambda > (700^4 + 575^4)^{1/4} \text{ GeV} = 769 \text{ GeV} , \quad (9)$$

which is consistent with our estimate in Eq. (8). It is clear that our estimate of the number of signal events is consistent with that of Ref. [9].

For $g_U = 1$ and $g_D = g_Q = 0$, we derive the following bound on Λ using the data and the SM background estimates of the ATLAS collaboration [10]:

$$\Lambda > 599 \text{ GeV} . \quad (10)$$

3.2 Study for $\sqrt{s} = 14$ TeV

In this subsection, we study the DM contribution and the SM background to the mono-jet cross section at the LHC with $\sqrt{s} = 14$ TeV. We introduce the following cut, which we refer to as *MonoJ14TeV*:

- Require $\cancel{E}_T > 800$ GeV.
- Highest p_T jet satisfies $|\eta_1| < 2.0$ and $p_{T1} > 700$ GeV.
- Event is vetoed if the second hardest jet satisfies $|\eta_2| < 4.5$, and $p_{T2} > 120$ GeV or $\Delta\phi(\vec{p}_{T2}, \vec{E}_T) < 0.5$.
- Event is vetoed if there is another jet that satisfies $|\eta| < 4.5$ and $p_T > 60$ GeV.
- Event is vetoed if there is an electron that satisfies $|\eta_e| < 2.47$ and $p_{Te} > 20$ GeV.
- Event is vetoed if there is a muon that satisfies $|\eta_\mu| < 2.4$ and $p_{T\mu} > 10$ GeV.

In comparison to the ATLAS *veryHighPT* selection cut, we keep the lepton veto conditions and scale all the jet p_T cuts by a factor of 2, while the \cancel{E}_T cut is chosen to reduce the $Z(\nu\nu) + \text{jet}$ background more efficiently in order to increase the signal significance for smaller DM signal cross sections.

We estimate the $Z(\nu\nu) + \text{jet}$ background in a manner similar to that for $\sqrt{s} = 7$ TeV, by changing the precuts to $\cancel{E}_T > 600$ GeV and $k_T > 240$ GeV for the jets, and the matching scale to 340 GeV. After testing the stability of our estimate under variation of the precuts and the matching scale, we find that the $Z + \text{jets}$ background cross section is given by

$$\sigma_{Z+\text{jets}}(\text{MonoJ14TeV}) = 12.8 \text{ fb} . \quad (11)$$

Similarly, we estimate the cross sections for the $W(\tau\nu) + \text{jet}$ and $W(l\nu) + \text{jet}$ backgrounds with the precuts $p_T^l > 600$ GeV and $k_T > 240$ GeV for the jets, and a matching scale of 340 GeV. We find

$$\sigma_{W(\tau\nu)+\text{jets}}(\text{MonoJ14TeV}) = 2.4 \text{ fb} , \quad (12)$$

$$\sigma_{W(l\nu)+\text{jets}}(\text{MonoJ14TeV}) = 2.4 \text{ fb} . \quad (13)$$

To estimate the DM signal contribution, we set $(g_Q, g_U, g_D) = (0, \cos\phi, \sin\phi)$ so that the magnitudes of the couplings are given by $1/\Lambda^2$, and the isospin violation is parametrized by the phase $-\pi/2 < \phi \leq \pi/2$. The up and down quark couplings have the same sign for $0 < \phi < \pi/2$,

m_χ	$\phi = 0$	$\phi = \pm\pi/4$	$\phi = \pm\pi/2$
10 GeV	15.9	11.0	6.37
300 GeV	15.1	10.5	5.91
500 GeV	13.0	8.89	4.98

Table 2: DM signal cross sections (in units of $(800 \text{ GeV}/\Lambda)^4 \text{ fb}$) for $\sqrt{s} = 14 \text{ TeV}$ with the *MonoJ14TeV* cut, for various values of the DM mass m_χ and the ratio of the DM couplings parametrized by $\phi = \tan^{-1}(g_D/g_U)$.

and opposite signs for $-\pi/2 < \phi < 0$. We repeat the simulation steps of the $\sqrt{s} = 7 \text{ TeV}$ case, by changing the precuts to $\cancel{E}_T > 600 \text{ GeV}$ and $k_T > 240 \text{ GeV}$ for the jets, and the matching scale to 340 GeV . We calculate the cross sections for various values of the DM mass m_χ and $\phi = \tan^{-1}(g_D/g_U)$; some of these are listed in Table 2 in units of $(800 \text{ GeV}/\Lambda)^4 \text{ fb}$. The mono-jet cross section does not distinguish between the signs of the g_U and g_D couplings, and hence $\pm\phi$ give the same prediction.

4 Mono-photon + \cancel{E}_T

The mono-jet cross section alone does not contain information on ϕ . Therefore additional signals are needed, and we study the mono-photon plus \cancel{E}_T signal in this section. Since the photon coupling to the up quark is twice that to the down quark, we expect a strong dependence of the DM signal on $|\phi|$. We first focus on the $\sqrt{s} = 7 \text{ TeV}$ case and reproduce the results of Ref. [9]. We then proceed to the $\sqrt{s} = 14 \text{ TeV}$ case, and look for an appropriate selection cut at high energies and at high integrated luminosity.

4.1 Study for $\sqrt{s} = 7 \text{ TeV}$

Following Refs. [9, 12], we implement the following selection cut, which we call *MonoG7TeV*:

- Require a photon with $|\eta_\gamma| < 1.44$ and $p_{T\gamma} > 95 \text{ GeV}$.
- Require $\cancel{E}_T > 80 \text{ GeV}$.
- Event is vetoed if there is a jet with $|\eta_j| < 3.0$ and $p_{Tj} > 20 \text{ GeV}$.
- Event is vetoed if there is an isolated lepton with $p_{Tl} > 10 \text{ GeV}$ and $\Delta R(l, \gamma) \equiv \sqrt{(\eta_l - \eta_\gamma)^2 + (\phi_l - \phi_\gamma)^2} > 0.04$.

The leading background arises from $Z(\nu\nu) + \gamma$ events. In addition, $Z(\nu\nu) + \text{jet}$ events with the jet misidentified as a photon, and $W(e\nu)$ events with the electron misidentified as a photon also contribute to the background.

We simulate the $Z(\nu\nu) + \gamma$ background as follows. We first generate $Z(\nu\nu) + \gamma$ and $Z(\nu\nu) + \gamma + 1 \text{ jet}$ events at the matrix element level with the precuts $p_{T\gamma} > 60 \text{ GeV}$ for the photon and $k_T > 60 \text{ GeV}$ for the jet, and simulate parton showering by using k_T -jet matching with a matching scale of 84 GeV. After simulating the detector effects with PGS and imposing the selection cut, we obtain

$$\sigma_{Z\gamma}(\text{Mono}G7TeV) = 48.0 \text{ fb} . \quad (14)$$

This gives 54.7 events in 1.14 fb^{-1} of data, while the CMS collaboration estimates 36.4 events [12]. We therefore multiply the DM signal (which has a similar event topology as the $Z(\nu\nu) + \gamma$ background) by the ratio $36.4/54.7 = 0.67$. This rescaling reflects the additional criteria for photon identification specific to the CMS detector. Note that the factor of 0.67 is in agreement with the analysis in Ref. [9], which finds 0.71.

The DM signal arises mainly from the following subprocesses:

$$u \bar{u} \rightarrow \gamma \chi \bar{\chi} , \quad (15)$$

$$d \bar{d} \rightarrow \gamma \chi \bar{\chi} . \quad (16)$$

Setting $m_\chi = 10 \text{ GeV}$ and $g_U = g_D = g_Q = 1$, we generate $\chi\bar{\chi} + \gamma$ and $\chi\bar{\chi} + \gamma + 1 \text{ jet}$ events at the matrix element level with the same precuts as for the background, which are then processed to the parton showering simulation with the same matching scale and finally the detector simulation is done using PGS. In this way, we find the DM signal cross section before the rescaling to be

$$\sigma_{DM\gamma}(\text{Mono}G7TeV) = 63.3 \times (400\text{GeV}/\Lambda)^4 \text{ fb} . \quad (17)$$

To compare our analysis with that of Ref. [9], we estimate the 90% C.L. lower bound on Λ by using the criterion of Eq. (7). For N_{SM} and σ_{SM} , we adopt the numbers estimated by the CMS collaboration, which are $N_{SM} = 67.3$ and $\sigma_{SM} = 8.4$ in 1.14 fb^{-1} [12]. The CMS collaboration reports $N_{obs} = 80$ [12]. N_{DM} is estimated by multiplying Eq. (17) by the normalization factor, 0.67. We obtain the 90% C.L. bound,

$$\Lambda > 422 \text{ GeV} . \quad (18)$$

On the other hand, Fig. 8 of Ref. [9] shows separate bounds on DM-up quark and DM-down quark interactions. These bounds can be translated into a bound on Λ for the case, $g_U = g_D =$

Cut	$\sigma_{Z\gamma}$	$\sigma_{DM\gamma}$	$\sigma_{DM\gamma}/\sqrt{\sigma_{Z\gamma} + \sigma_{DM\gamma}}$
<i>MonoG14TeV-a</i>	35.8	5.49	0.85
<i>MonoG14TeV-b</i>	11.6	3.34	0.87
<i>MonoG14TeV-c</i>	4.51	2.13	0.83

Table 3: Cross sections (in fb) and significance factors ($\text{fb}^{1/2}$) for the DM signal with $m_\chi = 10$ GeV, $\Lambda = 800$ GeV and $\phi = \pi/4$. The three selection cuts for mono-photon events are compared.

$g_Q = 1$:

$$\Lambda > (400^4 + 240^4)^{1/4} \text{ GeV} = 412 \text{ GeV} . \quad (19)$$

This is consistent with our result in Eq. (18).

4.2 Study for $\sqrt{s} = 14$ TeV

We introduce the following selection cut for the LHC with $\sqrt{s} = 14$ TeV, which we name *MonoG14TeV-a*:

- Require a photon with $|\eta_\gamma| < 1.44$ and $p_{T\gamma} > 140$ GeV.
- Require $\cancel{E}_T > 140$ GeV.
- Event is vetoed if there is a jet with $|\eta_j| < 3.0$ and $p_{Tj} > 40$ GeV.
- Event is vetoed if there is an isolated lepton with $p_{Tl} > 10$ GeV and $\Delta R(l, \gamma) > 0.04$.

We also introduce the selection cut *MonoG14TeV-b* which requires $(p_{T\gamma}, \cancel{E}_T) > (200, 200)$ GeV, and the cut *MonoG14TeV-c* which requires $(p_{T\gamma}, \cancel{E}_T) > (260, 260)$ GeV, and for which all the other requirements are the same as for *MonoG14TeV-a*.

We estimate the $Z(\nu\nu) + \gamma$ background in a similar manner to the case of $\sqrt{s} = 7$ TeV, by changing the precuts to $p_{T\gamma} > 100$ GeV for the photon and $k_T > 100$ GeV for the jet, and the matching scale to 140 GeV. We estimate the DM signal contribution with the same precuts and matching scale as for the $Z(\nu\nu) + \gamma$ background estimation for $\sqrt{s} = 14$ TeV.

Table 3 shows the cross sections and significance factors ($S/\sqrt{S+B}$) for the DM signal with $m_\chi = 10$ GeV, $\Lambda = 800$ GeV and $\phi = \pi/4$, where the three selection cuts are imposed. The numbers are in units of fb for the cross sections and $\text{fb}^{1/2}$ for the significance factor. We find that the significance factor does not depend much on the choice of the selection cut. This is because the background cross section decreases by a factor of 8 and the signal also decreases

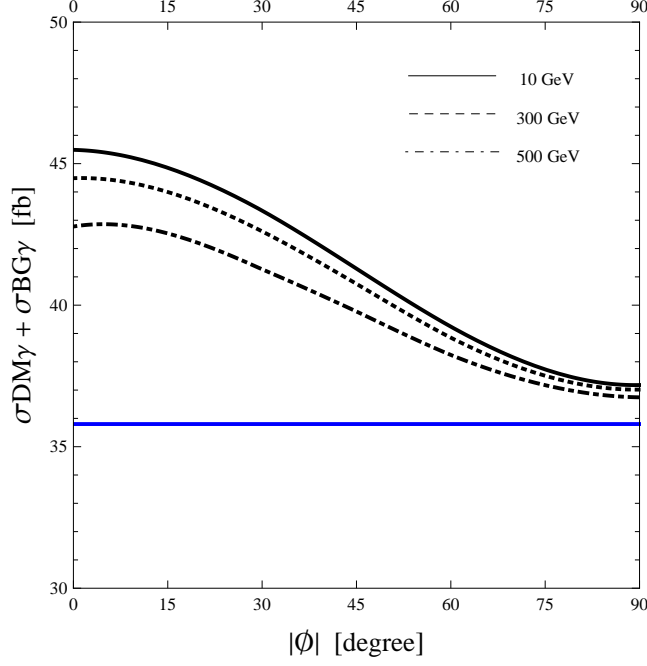


Figure 2: The $Z + \gamma$ background cross section and the DM signal cross section for $\Lambda = 800$ GeV that satisfy the *MonoG14TeV-a* criteria, as a function of $|\phi|$ for the couplings $(g_Q, g_U, g_D) = (0, \cos \phi, \sin \phi)$. The horizontal solid line corresponds to the background cross section. The curves correspond to the background + signal cross sections for three values of m_χ .

by $2.6 \simeq \sqrt{8}$ when we change the cut from *MonoG14TeV-a* to *MonoG14TeV-c*. For our study, we adopt the selection cut *MonoG14TeV-a* which yields the largest signal cross section. This is because, with more events, it is easier to discriminate the signal from the background from the difference in their \cancel{E}_T and $p_{T\gamma}$ distributions as well as from the correlation between γ and \cancel{E}_T momenta, although we do not perform such an analysis in this paper.

In Fig. 2, we show the cross sections for the $Z + \gamma$ background and the DM signal for $\Lambda = 800$ GeV and $(g_Q, g_U, g_D) = (0, \cos \phi, \sin \phi)$ that satisfy the cut *MonoG14TeV-a*. The three curves correspond to $m_\chi = 10, 300, 500$ GeV. The mono-photon cross section does not depend on the signs of the g_U and g_D couplings, and hence $\pm\phi$ give the same prediction.

In Table 4, we present the DM signal cross sections in units of $(800 \text{ GeV}/\Lambda)^4 \text{ fb}$ for three representative couplings, $\phi = 0$ ($g_U = 1$), $\phi = \pm\pi/4$ ($|g_U| = |g_D| = 1/\sqrt{2}$) and $\phi = \pi/2$ ($g_D = 1$). Roughly speaking, the $\phi = \pi/2$ ($g_D = 1$) case gives about a factor of 7 smaller DM signal cross section than the $\phi = 0$ ($g_U = 1$) case, while the cross section in the $\phi = \pm\pi/4$ ($|g_U| = |g_D| = 1/\sqrt{2}$) case is about half of that in the $\phi = 0$ case, for all m_χ between 10 GeV and 500 GeV. This reflects the combined effect of the QED coupling ratio $(Q_d/Q_u)^2 = 1/4$ and the ratio of the down quark to up quark parton distribution functions in pp collisions.

m_χ	$\phi = 0$	$\phi = \pm\pi/4$	$\phi = \pm\pi/2$
10 GeV	9.69	5.49	1.38
300 GeV	8.69	4.96	1.22
500 GeV	6.98	3.98	0.945

Table 4: DM signal cross sections (in units of $(800 \text{ GeV}/\Lambda)^4 \text{ fb}$) for $\sqrt{s} = 14 \text{ TeV}$ that satisfy the *MonoG14TeV-a* cut.

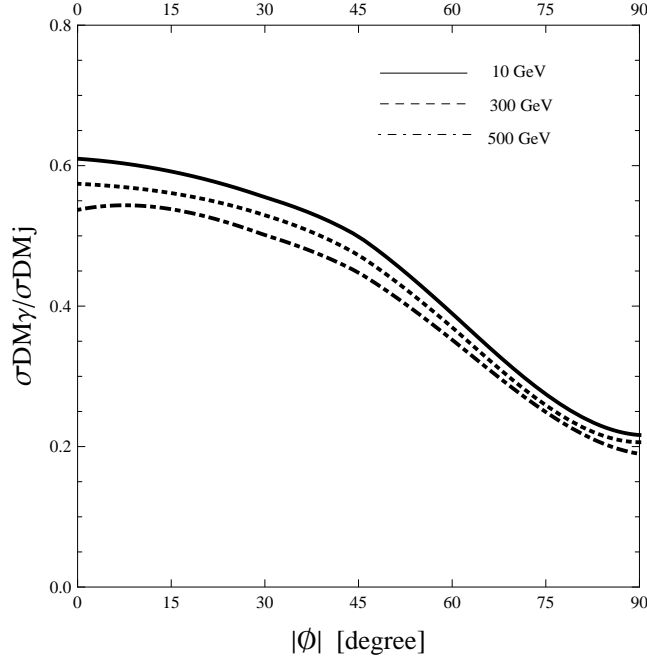


Figure 3: Ratio of the DM signal cross section in the mono-photon channel with the *MonoG14TeV-a* cut to the cross section in the mono-jet channel with the *MonoJ14TeV* cut for three values of m_χ .

In Fig. 3, we show the ratio of the DM signal cross sections in the mono-photon channel with the *MonoG14TeV-a* cut to the cross section in the mono-jet channel with the *MonoJ14TeV* cut. We find that this ratio is very sensitive to the coupling ratio $|g_D/g_U| = \tan|\phi|$, but insensitive to the DM mass m_χ . It is independent of Λ and $\sqrt{g_U^2 + g_D^2}$.

Experimentally, the cross section ratio, $\sigma_{DM}^\gamma/\sigma_{DM}^j$, is determined by

$$\frac{\sigma_{DM}^\gamma(\text{monophoton cut})}{\sigma_{DM}^j(\text{monojet cut})} = \frac{(N_{obs}^\gamma - N_{SM}^\gamma)(\text{monophoton cut})}{(N_{obs}^j - N_{SM}^j)(\text{monojet cut})}, \quad (20)$$

where N_{obs}^γ and N_{obs}^j are the observed number of mono-photon and mono-jet events, respectively, and N_{SM}^γ and N_{SM}^j are the SM expectations for mono-photon background events and mono-jet background events, respectively. Since the cross section ratio has a common value for a wide

range of m_χ , we can determine the value of $|\phi|$ by comparing the observed value of the cross section ratio with Fig. 3.

As an illustration, we estimate the integrated luminosity L needed to measure the cross section ratio with 10% accuracy close to the point $|\phi| = \pi/4$ for $\Lambda = 800$ GeV and $m_\chi = 10$ GeV. We assume that the statistical uncertainty of the number of events, N , follows $\Delta N = \sqrt{N}$, and ignore systematic uncertainties. To estimate N_{obs}^γ and N_{SM}^γ , we rescale the cross sections by the normalization factor 0.67 obtained in Section 4.1. The statistical uncertainty of $\sigma_{DM\gamma}/\sigma_{DMj}$ is given by

$$\Delta \left(\frac{\sigma_{DM}^\gamma}{\sigma_{DM}^j} \right) = \left(\frac{\sigma_{DM}^\gamma}{\sigma_{DM}^j} \right) \sqrt{ \frac{N_{obs}^j + N_{SM}^j}{(N_{obs}^j - N_{SM}^j)^2} + \frac{N_{obs}^\gamma + N_{SM}^\gamma}{(N_{obs}^\gamma - N_{SM}^\gamma)^2} } . \quad (21)$$

Inserting $N_{SM}^\gamma = L \times 0.67 \times 35.8$ fb and $N_{obs}^\gamma - N_{SM}^\gamma = L \times 0.67 \times 5.49$ fb from Table 3, $N_{SM}^j = L \times (12.8 + 2.4 + 2.4)$ fb from Eqs. (11-13), and $N_{obs}^j - N_{SM}^j = L \times 11.0$ fb from Table 2, we find that in order to obtain a 10% measurement of the monophoton-to-monojet cross section ratio, $L \simeq 420$ fb $^{-1}$ is needed.

5 Di-jet + \cancel{E}_T

Since the mono-jet and mono-photon cross sections depend only on the absolute values of g_U and g_D , a measurement of the relative sign of g_U and g_D is not possible from these channels. To determine the relative sign, we now focus on events with two hard jets and large \cancel{E}_T . This channel can be sensitive to the relative sign of the g_U and g_D couplings because in the subprocess,

$$u_R d_R \rightarrow u_R d_R \chi \bar{\chi} , \quad (22)$$

the amplitudes where $\chi \bar{\chi}$ are emitted from the up quark interfere with the amplitudes where $\chi \bar{\chi}$ are emitted from the down quark, as can be seen from the Feynman diagrams in Fig. 4. The interference term is directly proportional to $g_U g_D$ so that the cross section depends on the sign of $g_U g_D$.

5.1 Extracting the Interference

In this subsection we discuss kinematic conditions that enhance interference effects in the diagrams of Fig. 4.

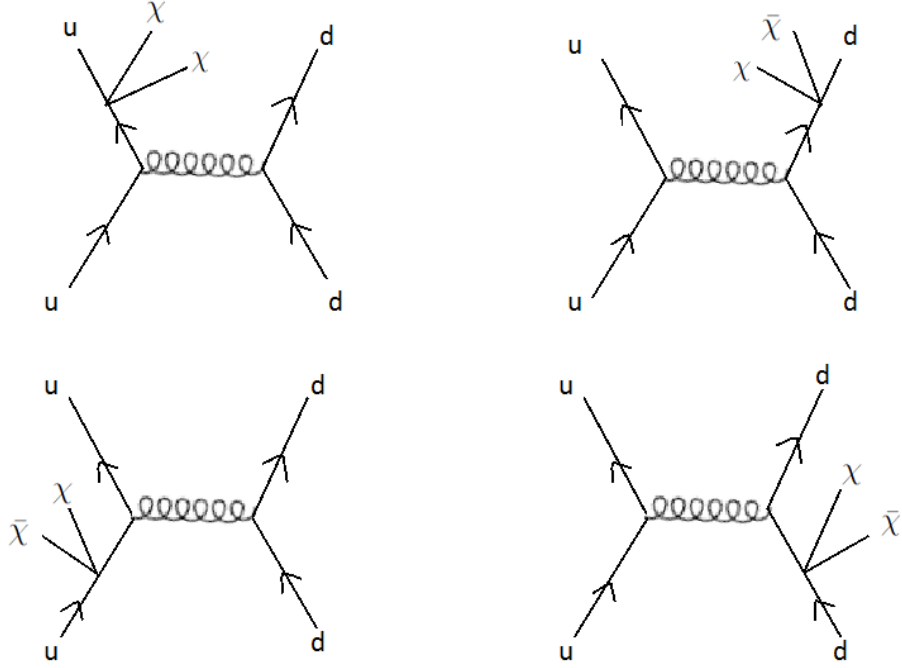


Figure 4: Feynman diagrams for the subprocess, $u_R d_R \rightarrow u_R d_R \chi \bar{\chi}$. The diagrams on the left are proportional to g_U , and the ones on the right are proportional to g_D .

5.1.1 Suppressing contributions from quark-gluon collisions

First, it is necessary to suppress large contributions from quark-gluon collisions,

$$q g \rightarrow q g Z(\nu\nu), \quad (23)$$

$$q g \rightarrow q g \chi \bar{\chi}, \quad (q = u, d). \quad (24)$$

While the subprocesses in Eq. (23) give the dominant background for the DM plus di-jet production events, the subprocesses in Eq. (24) should also be suppressed because their cross sections do not depend on $g_U g_D$. The contributions from quark-gluon collisions can be reduced, compared to the signal subprocess in Eq. (22) from quark-quark collisions by imposing a very large cut on the “di-jet cluster transverse mass” [13]:

$$M_T(jj; \cancel{E}_T) \equiv \sqrt{M_{12}^2 + |\vec{p}_{1T} + \vec{p}_{2T}|^2} + \cancel{E}_T, \quad (25)$$

where M_{12} is the invariant mass of the two hardest jets, and $\vec{p}_{1T} + \vec{p}_{2T}$ is the vector sum of the transverse momenta of the two hardest jets. Since the parton center-of-mass energy ($\sqrt{\hat{s}}$) is always larger than $M_T(jj; \cancel{E}_T)$, by imposing a cut on $M_T(jj; \cancel{E}_T)$, we can select those events that satisfy

$$\sqrt{\hat{s}} \geq M_T(jj; \cancel{E}_T) > (M_T(jj; \cancel{E}_T))^{\text{cut}}. \quad (26)$$

By choosing a large value for $(M_T(jj; \cancel{E}_T))^{cut}$, we can suppress the contributions from quark-gluon collisions relative to those from quark-quark collisions, because the former subprocesses have relatively less parton center-of-mass energy. We note that the contributions from the same quark collisions:

$$q q \rightarrow q q Z(\nu\nu) , \quad (27)$$

$$q q \rightarrow q q \chi\bar{\chi} , \quad (q = u, d), \quad (28)$$

cannot be suppressed by a cut on $M_T(jj; \cancel{E}_T)$. We therefore treat them as irreducible backgrounds for a measurement of the sign of $g_U g_D$.

5.1.2 Utilizing the generalized null radiation zone theorem

Generally speaking, when a subprocess contains two Feynman diagrams that interfere, the ratio of the interference term to the cross section is maximized when the amplitudes of the two diagrams take the same absolute value. The null radiation zone theorem [14] provides us with powerful criteria for identifying such kinematic regions. The theorem states that for any tree-level Feynman diagram, if the ratio $Q_k/(p_k \cdot q)$ (where Q_k is the charge of an external particle, p_k is its four-momentum, and q is the four-momentum of the emitted photon) is the same for all external particles and if the charge Q_k 's are conserved, then the sum of the amplitudes of all the tree-level diagrams made by adding one photon emission vertex to the original diagram vanishes for all helicities. Since the amplitude for each diagram does not vanish, the theorem implies that the amplitudes of the contributing diagrams cancel exactly, *i.e.*, they interfere maximally. The original theorem applies to massless vector boson emission via a vector coupling to fermions. We make use of the theorem for our dark matter pair which couples to quarks via vector and axial vector couplings. Since the dark matter pair is not massless, we first generalize the theorem to emission of a massive vector current.

We now show that the null radiation zone theorem can be generalized to emission of a massive vector boson, or a vector current whose invariant mass squared is time-like, $q^2 > 0$. Consider the following process in which a neutral vector current, V , is emitted:

$$a + b \rightarrow 1 + 2 + \dots + n + V . \quad (29)$$

We label the particle four-momenta and charges in the initial state by p_i , Q_i ($i = a, b$), and those in the final state by p_f , Q_f ($f = 1, 2, \dots, n$). We denote the four-momentum of the vector current by q . The tree-level scattering amplitude should vanish for all helicities when

the following conditions are satisfied:

$$\frac{Q_i}{2p_i \cdot q - q^2} = \frac{Q_f}{2p_f \cdot q + q^2} = (\text{a common value}) \quad \text{for all } i \text{ and } f, \quad (30)$$

$$\sum_i Q_i = \sum_f Q_f. \quad (31)$$

Let us focus on the four diagrams of Fig. 4. We denote the four-momenta of the incoming quarks by k_1 and k_2 , those of the outgoing quarks by p_1 and p_2 and the four-momentum sum of the DM momenta by q . We notice that the values of $2p_1 \cdot q + q^2$ and $2p_2 \cdot q + q^2$ are always positive. The values of $2k_1 \cdot q - q^2$ and $2k_2 \cdot q - q^2$ can take both signs, but their sum is always positive because $k_1 + k_2 = p_1 + p_2 + q$. Therefore the null radiation zone can be realized only when g_U and g_D take the same sign. We thus expect that the interference in pp collisions is destructive if g_U and g_D take the same sign, and is constructive otherwise.

The theorem suggests that if the condition,

$$k_1 \cdot q - \frac{q^2}{2} = k_2 \cdot q - \frac{q^2}{2} = p_1 \cdot q + \frac{q^2}{2} = p_2 \cdot q + \frac{q^2}{2}, \quad (32)$$

is satisfied, the amplitudes of the four diagrams of Fig. 4 cancel completely for $g_U = g_D$, while the sum of the amplitudes is maximally enhanced for $g_U = -g_D$. Equation (32) reduces to the following kinematic conditions for massless partons satisfying $p_1^2 = p_2^2 = k_1^2 = k_2^2 = 0$:

$$|\vec{p}_1| = |\vec{p}_2|, \quad (33)$$

$$q^2 = 0, \quad (34)$$

where $|\vec{p}_1|$ and $|\vec{p}_2|$ are respectively the magnitudes of the three-momenta of p_1 and p_2 in the *colliding parton center-of-mass* frame. Since our DM particle is not massless, the condition Eq. (32) cannot be satisfied and the null radiation zone does not exist in the physical region. However, we expect that strong destructive interference occurs for $g_U = g_D$ when the condition Eq. (32) is approximately satisfied.

At hadron colliders, we cannot measure the missing mass $\sqrt{q^2}$, and cannot determine the colliding parton center-of-mass frame. Therefore, to enhance kinematic regions around the null radiation zone, we must make use of the constraints among jet transverse momenta coming from Eq. (33). In the following we examine the selection cut,

$$|p_{T1} - p_{T2}| < C p_{T1}, \quad (35)$$

where p_{T1} and p_{T2} are the transverse momenta of the hardest and second hardest jets, respectively, and C is a number less than unity. Although no selection cut can be applied to enhance kinematic regions that nearly satisfy Eq. (32), such regions are automatically favored in pp collisions with a fixed cut because they are the regions where the parton center-of-mass energy is minimized.

5.2 Analysis

The “signal” in this analysis is not DM production itself, but the difference in the DM signal cross sections for $g_U/g_D > 0$ and $g_U/g_D < 0$. In this analysis, therefore, we consider the value of $\sigma_{DMjj}(\phi = -\pi/4) - \sigma_{DMjj}(\phi = \pi/4)$ as the signal and treat the value of $\sigma_{DMjj}(\phi = -\pi/4) + \sigma_{SM}$ as the background.

We first examine selection cuts dubbed *DiJ-a*, *DiJ-b*, *DiJ-c* and *DiJ-d*. The *DiJ-a* cut is:

- Require two jets with $|\eta| < 4.5$ and $p_T > 200$ GeV.
- Require $\cancel{E}_T > 300$ GeV.
- Require $M_T(jj; \cancel{E}_T) = \sqrt{M_{12}^2 + |\vec{p}_{1T} + \vec{p}_{2T}|^2} + \cancel{E}_T > 2$ TeV.
- Event is vetoed if there is another jet that satisfies $|\eta| < 4.5$ and $p_T > 100$ GeV.
- Event is vetoed if there is a jet whose three-momentum \vec{p} satisfies $\Delta\phi(\vec{p}, \vec{\cancel{E}}_T) < 0.2$.

The first, second and fourth conditions define the two jets plus large \cancel{E}_T events that we study. It is the third condition that enhances events from quark-quark collisions over those from quark-gluon collisions. The last condition is necessary to reduce those $Z(\nu\nu) + \text{jets}$ events in which a quark emits the Z boson almost collinearly; the amplitude receives collinear enhancement even for the Z boson because $E_{jet}/M_Z \gg 1$. For comparison, we consider a selection cut *DiJ-b* that requires $M_T(jj; \cancel{E}_T) > 2.5$ TeV, and a selection cut *DiJ-c* that requires $M_T(jj; \cancel{E}_T) > 3$ TeV, with the other conditions the same as for *DiJ-a*. Based on the null radiation zone theorem, we also consider a selection cut *DiJ-d* that requires

$$|p_{T1} - p_{T2}| < 0.5 p_{T1}, \quad (36)$$

in addition to the conditions of *DiJ-b*. (p_{T1} and p_{T2} are the transverse momenta of the hardest and second hardest jets, respectively.) The cuts are summarized as follows:

$$DiJ - a : M_T(jj; \cancel{E}_T) > 2 \text{ TeV} . \quad (37)$$

$$DiJ - b : M_T(jj; \cancel{E}_T) > 2.5 \text{ TeV} . \quad (38)$$

$$DiJ - c : M_T(jj; \cancel{E}_T) > 3 \text{ TeV} . \quad (39)$$

$$DiJ - d : M_T(jj; \cancel{E}_T) > 2.5 \text{ TeV} \quad \text{and} \quad |p_{T1} - p_{T2}| < 0.5 p_{T1} . \quad (40)$$

Our simulation of the SM background only accounts for the dominant background from $Z(\nu\nu) + \text{jets}$ events. To estimate the background cross section, we generate $Z(\nu\nu) + 2, 3$ jets events at the matrix element level with the following precuts: $\cancel{E}_T > 200$ GeV, $k_T > 160$ GeV,

Cut	σ_{Zjj}	$\sigma_{DMjj}(\phi = \frac{\pi}{4})$	$\sigma_{DMjj}(\phi = -\frac{\pi}{4})$	$\frac{\sigma_{DMjj}(-\pi/4) - \sigma_{DMjj}(\pi/4)}{\sigma_{DMjj}(-\pi/4)}$	$\frac{\sigma_{DMjj}(-\pi/4) - \sigma_{DMjj}(\pi/4)}{\sqrt{\sigma_{Zjj} + \sigma_{DMjj}(-\pi/4)}}$
<i>DiJ-a</i>	49.8	9.246	9.595	0.0364	0.0453
<i>DiJ-b</i>	20.1	4.094	4.355	0.0599	0.0528
<i>DiJ-c</i>	8.34	1.868	1.999	0.0655	0.0407
<i>DiJ-b</i>	13.7	1.847	2.012	0.0820	0.0416

Table 5: Cross sections (in fb), the dimensionless ratio of the interference effect to the DM production cross section, and the significance factor ($\text{fb}^{1/2}$) for DM production with $m_\chi = 10$ GeV, $\Lambda = 800$ GeV and $\phi = \pm\pi/4$, for four different cuts.

$\Delta R(\vec{p}_j, \vec{p}_Z) > 0.2$, $\sqrt{\hat{s}} > 2$ (2.5) TeV when using the *DiJ-a* cut (*DiJ-b*, *DiJ-c* and *DiJ-d* cuts), where \vec{p}_j is the three-momentum of any jet and \vec{p}_Z that of the Z boson. We match the matrix element events with the parton shower with a matching scale of 220 GeV, and perform a detector simulation. We find that the cross section after the final cut does not change drastically when the matching scale is varied by ± 40 GeV.

The DM production cross section is estimated in a similar manner; we generate $\chi\bar{\chi} + 2, 3$ jets events with the same precuts as the background simulation (\vec{p}_Z is replaced with the three-momentum sum of the DM momenta), and process them to parton showering and detector simulation with the same matching scale.

Table 5 shows the cross sections and the significance factors ($S/\sqrt{S+B}$) for DM production with $m_\chi = 10$ GeV, $\Lambda = 800$ GeV and $\phi = \pm\pi/4$, for the four selection cuts. Also shown is the ratio of the interference effect ($\sigma_{DMjj}(\phi = -\pi/4) - \sigma_{DMjj}(\phi = +\pi/4)$) to the DM production cross section for $\phi = -\pi/4$ ($\sigma_{DMjj}(\phi = -\pi/4)$). Notice that in this analysis the “signal” cross section corresponds to the difference between the DM cross sections for $\phi = \pi/4$ and $\phi = -\pi/4$. The numbers are in units of fb for the cross sections and $\text{fb}^{1/2}$ for the significance factors. From Table 5 we see that the *DiJ-b* cut gives the largest significance factor. We note in passing that the requirement Eq. (36) of the *DiJ-d* cut, which is based on the null radiation zone theorem, does enhance the ratio of the interference effect to the DM production cross section, $\{\sigma_{DMjj}(\phi = -\pi/4) - \sigma_{DMjj}(\phi = +\pi/4)\}/\sigma_{DMjj}(\phi = -\pi/4)$. Unfortunately, the $Z +$ jets background is not significantly diminished by this requirement, resulting in a significance factor that is smaller for the *DiJ-d* cut than for the *DiJ-b* cut.

In Fig. 5 and Table 6, we show cross sections for the $Z +$ jets background and the DM production process for $\Lambda = 800$ GeV and $m_\chi = 10, 300$ GeV that satisfy the *DiJ-b* selection cut. The numbers in the table are in units of $(800 \text{ GeV}/\Lambda)^4 \text{ fb}$. Finally in Fig. 6, we show the ratio of the DM signal cross section in the di-jet channel with the *DiJ-b* cut to the cross section in the mono-jet channel with the *MonoJ14TeV* cut, as a function of ϕ .

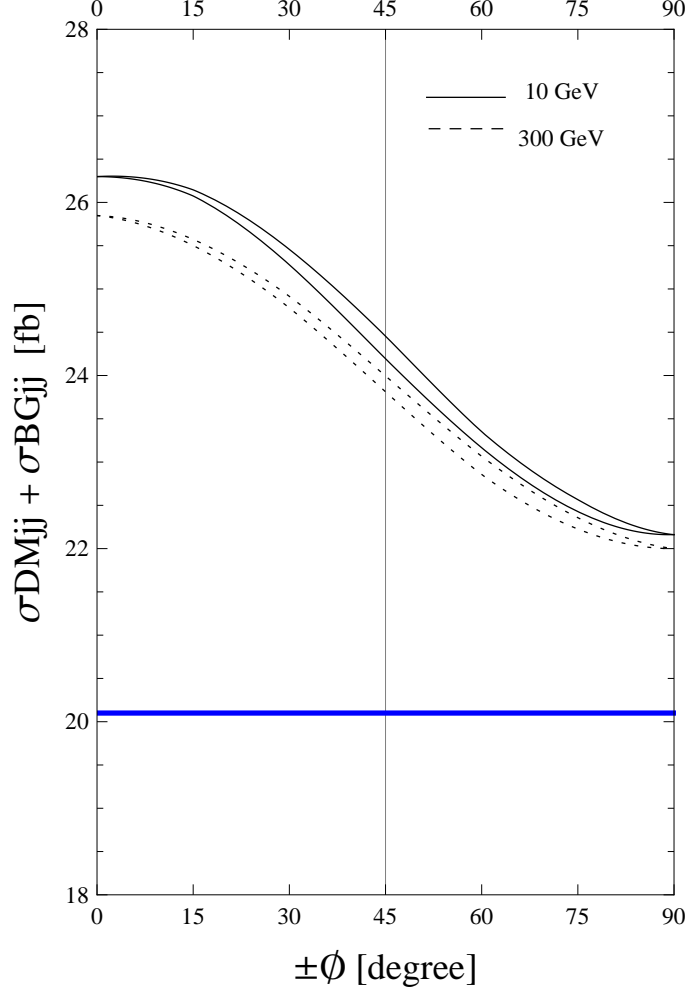


Figure 5: The $Z + \text{jets}$ background cross section and the DM production cross section for $\Lambda = 800 \text{ GeV}$ that satisfy the $DiJ\text{-}b$ selection cut, as a function of ϕ for the couplings $(g_Q, g_U, g_D) = (0, \cos \phi, \sin \phi)$. The horizontal solid line corresponds to the background cross section. The solid and dotted curves correspond to the background + signal cross sections for $m_\chi = 10 \text{ GeV}$ and 300 GeV , respectively. For each pair of curves, the upper one corresponds to $\phi < 0$ and the lower one to $\phi > 0$.

m_χ	$\phi = +\pi/4$	$\phi = -\pi/4$
10 GeV	4.094	4.355
300 GeV	3.712	3.895

Table 6: DM production cross sections (in units of $(800 \text{ GeV}/\Lambda)^4 \text{ fb}$) for $\sqrt{s} = 14 \text{ TeV}$ that satisfy the $DiJ\text{-}b$ selection cut.

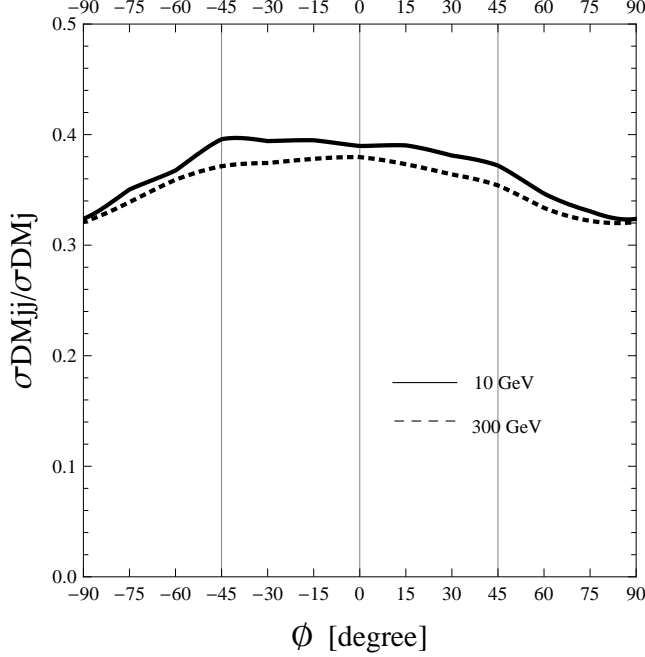


Figure 6: Ratio of the DM production cross section in the di-jet channel with the *DiJ-b* cut to the cross section in the mono-jet channel with the *MonoJ14TeV* cut for two values of m_χ .

5.3 Discussion of the Di-jet Channel

From Fig. 5 and Table 6, we confirm that the Feynman diagrams of the subprocess, $u_R d_R \rightarrow \chi \bar{\chi} u_R d_R$, interfere destructively if g_U and g_D have the same sign, and constructively if they have opposite signs. This is in accordance with our expectation in Section 5.1 based on the null radiation zone theorem [14]. Table 6 also indicates that the effect of the interference is diminished for larger DM masses. This is because for heavier DM, the physical region deviates more from the null radiation zone given by Eq. (32).

The deviation of Fig. 6 from a left-right symmetric form is a consequence of the interference. Apart from the left-right asymmetry, Fig. 6 shows that the cross section ratio is smaller for $\phi \simeq \pm\pi/2$ than for $\phi \simeq 0$. This is due to the difference in the parton distribution functions of the up and down quarks; since the momentum distribution of the down quark in a proton leans towards a smaller momentum region compared to that of the up quark, events involving only down quarks have relatively less parton center-of-mass energy and are more likely to be rejected by the high cut on $M_T(jj; \cancel{E}_T)$.

Once it has been experimentally established that $|g_U| \simeq |g_D|$ ($|\phi| \simeq \pi/4$), and that $m_\chi \sim 10$ GeV, the sign of $g_U g_D$ can be determined by measuring the following DM cross section

ratio and comparing it with the prediction of Fig. 6:

$$\frac{\sigma_{DM}^{jj}}{\sigma_{DM}^j} = \frac{(N_{obs}^{jj} - N_{SM}^{jj})(DiJ-b)}{(N_{obs}^j - N_{SM}^j)(MonoJ14TeV)} , \quad (41)$$

where N_{obs}^{jj} is the observed number of di-jet events and N_{SM}^{jj} is the SM expectation for di-jet events.

We estimate the integrated luminosity needed to determine the sign of $g_U g_D$ for $\Lambda = 800$ GeV, $m_\chi = 10$ GeV and $|\phi| = \pi/4$. To distinguish $\phi = -\pi/4$ from $\phi = +\pi/4$ at the 2σ level, the dijet-to-monojet cross section ratio must be measured with 3% accuracy since Table 5 shows that the difference between the 2 cases is about 6%. The statistical uncertainty of $\sigma_{DMjj}/\sigma_{DMj}$ is given by

$$\Delta \left(\frac{\sigma_{DMjj}}{\sigma_{DMj}} \right) = \left(\frac{\sigma_{DMjj}}{\sigma_{DMj}} \right) \sqrt{\frac{N_{obs}^j + N_{SM}^j}{(N_{obs}^j - N_{SM}^j)^2} + \frac{N_{obs}^{jj} + N_{SM}^{jj}}{(N_{obs}^{jj} - N_{SM}^{jj})^2}} . \quad (42)$$

Inserting $N_{SM}^{jj} = L \times 20.1$ fb and $N_{obs}^{jj} - N_{SM}^{jj} = L \times 4.355$ fb from Table 5, and $N_{SM}^j = L \times (12.8 + 2.4 + 2.4)$ fb from Eqs. (11-13) and $N_{obs}^j - N_{SM}^j = L \times 11.0$ fb from Table 2, we find that to achieve a 3% measurement of the dijet-to-monojet cross section ratio, $L \simeq 3000 \text{ fb}^{-1}$ is needed.

6 Conclusions

We explored ways of observing the isospin violating nature of a dark matter particle at the LHC. We adopted a Dirac fermion DM particle that couples to up and down quarks through contact interactions with different strengths. The cross section ratio of the DM production associated with a hard jet and that with a photon reflects the absolute value of the ratio of the DM couplings to up and down quarks because they have different electric charges. We showed that this ratio can be measured at the LHC by observing and comparing mono-photon + \cancel{E}_T events with mono-jet + \cancel{E}_T events.

The relative sign of the DM couplings to up and down quarks can be studied only by comparing the cross section of DM production associated with two hard jets to that with one hard jet. This is because the subprocess, $u_R d_R \rightarrow u_R d_R \chi \bar{\chi}$, that contributes to di-jet + \cancel{E}_T events, contains an interference term that is proportional to $g_U g_D$. In order to extract the interference term, we implemented a very hard cut on the di-jet cluster transverse mass, $M_T(jj; \cancel{E}_T)$, which selects quark-quark collision events over quark-gluon collision backgrounds. We showed that the effect of the interference does in fact appear in the cross section of di-jet + \cancel{E}_T events with

the sign expected from the null radiation zone theorem [14], and that it is possible to determine the relative sign of the couplings by observing and comparing di-jet + \cancel{E}_T events with mono-jet + \cancel{E}_T events.

Throughout, we focused on the case with $g_Q = 0$. If $g_Q \neq 0$, the DM cross section ratios in Figs. 3 and 6, will be modified. For Fig. 3, the angle ϕ will be replaced by

$$\phi_{eff} = \tan^{-1} \left(\sqrt{g_D^2 + g_Q^2} / \sqrt{g_U^2 + g_Q^2} \right) .$$

On the other hand, Fig. 6 will be modified in a complicated way. Note that the ratio of the di-jet and mono-jet signal cross sections can be written in the following way when $g_Q = 0$:

$$\sigma_{jj}/\sigma_j = \frac{Cg_U^2 + Dg_Ug_D + Eg_D^2}{Ag_U^2 + Bg_D^2} , \quad (43)$$

where A, B, C, D, E are numerical factors with $A, B, C, E > 0$ and $D < 0$ as we saw in Section 5. For $g_Q \neq 0$, the expression above becomes:

$$\sigma_{jj}/\sigma_j = \frac{C(g_U^2 + g_Q^2) + D(g_Ug_D + g_Qg_U + g_Qg_D) + E(g_D^2 + g_Q^2)}{A(g_U^2 + g_Q^2) + B(g_D^2 + g_Q^2)} . \quad (44)$$

Our analysis can be generalized to the entire parameter space of (g_Q, g_U, g_D) .

Although this work is motivated by isospin violating dark matter, our methods are applicable to other new physics models for which one studies the ratio of the new physics couplings to up and down quarks. The di-jet channel is challenging because it is necessary to suppress large contributions from gluon-quark interactions. However, it is the only channel that is sensitive to the relative sign of the up and down quark couplings, and hence should be studied seriously once new physics that couples to quarks is discovered. We believe that our exploratory studies will turn out to be useful to probe new physics properties at the LHC.

Acknowledgments

D.M. thanks the KEK Theory Center, where this work was initiated, for its support and hospitality. He also thanks the Center for Theoretical Underground Physics and Related Areas (CETUP* 2012) in South Dakota for its support and hospitality during the completion of this work. T.Y. thanks the organizers and the lecturers of “KIAS School on MadGraph for LHC Physics Simulation” (24-29 October, 2011) [15], where physics simulation tools used in this study were introduced. This work was supported in part by Grant-in-Aids for Scientific Research (Nos. 23-3599, 20340064 and 23104006) from the Japan Society for the Promotion of Science, and by US DOE grant DE-FG02-04ER41308 and US NSF grant PHY-0544278.

References

- [1] J. L. Feng, J. Kumar, D. Marfatia and D. Sanford, Phys. Lett. B **703**, 124 (2011) [arXiv:1102.4331 [hep-ph]].
- [2] R. Bernabei *et al.* [DAMA Collaboration], Eur. Phys. J. C **56**, 333 (2008) [arXiv:0804.2741 [astro-ph]].
- [3] C. E. Aalseth *et al.* [CoGeNT Collaboration], Phys. Rev. Lett. **106**, 131301 (2011) [arXiv:1002.4703 [astro-ph.CO]].
- [4] E. Aprile, *et al.* [XENON100 Collaboration], arXiv:1207.5988 [astro-ph.CO]; Phys. Rev. Lett. **107**, 131302 (2011) [arXiv:1104.2549 [astro-ph.CO]]; J. Angle *et al.* [XENON10 Collaboration], Phys. Rev. Lett. **107**, 051301 (2011) [arXiv:1104.3088 [astro-ph.CO]].
- [5] D. S. Akerib *et al.* [CDMS Collaboration], Phys. Rev. D **82**, 122004 (2010) [arXiv:1010.4290 [astro-ph.CO]]; Z. Ahmed *et al.* [CDMS-II Collaboration], Phys. Rev. Lett. **106**, 131302 (2011) [arXiv:1011.2482 [astro-ph.CO]].
- [6] J. Alwall, P. Demin, S. de Visscher, R. Frederix, M. Herquet, F. Maltoni and T. Plehn *et al.*, JHEP **0709**, 028 (2007) [arXiv:0706.2334 [hep-ph]]; J. Alwall, M. Herquet, F. Maltoni, O. Mattelaer and T. Stelzer, JHEP **1106**, 128 (2011) [arXiv:1106.0522 [hep-ph]].
- [7] T. Sjostrand, S. Mrenna and P. Z. Skands, JHEP **0605**, 026 (2006) [hep-ph/0603175].
- [8] J. Conway *et al.*, PGS (Pretty Good Simulation), <http://physics.ucdavis.edu/~conway/research/software/pgs/pgs4-general.htm>
- [9] P. J. Fox, R. Harnik, J. Kopp and Y. Tsai, Phys. Rev. D **85**, 056011 (2012) [arXiv:1109.4398 [hep-ph]].
- [10] G. Aad *et al.* [ATLAS Collaboration], Phys. Lett. B **705**, 294 (2011) [arXiv:1106.5327 [hep-ex]]; Tech. Rep. ATLAS-CONF-2011-096, CERN, Geneva (2011).
- [11] M. L. Mangano, M. Moretti and R. Pittau, Nucl. Phys. B **632**, 343 (2002) [hep-ph/0108069]; M. L. Mangano, M. Moretti, F. Piccinini and M. Treccani, JHEP **0701**, 013 (2007) [hep-ph/0611129].
- [12] S. Chatrchyan *et al.* [CMS Collaboration], Phys. Rev. Lett. **107**, 201804 (2011) [arXiv:1106.4775 [hep-ex]]; Tech. Rep. CMS-PAS-EXO-11-059, CERN, Geneva (2011).

- [13] V. D. Barger, A. D. Martin and R. J. N. Phillips, Phys. Lett. B **125**, 339 (1983).
- [14] R. W. Brown, K. L. Kowalski and S. J. Brodsky, Phys. Rev. D **28**, 624 (1983).
- [15] KIAS School on MadGraph for LHC Physics Simulation (24-29, October 2011, KIAS, Seoul, <http://workshop.kias.re.kr/MGLP>).